Thermodynamically adaptive piecewise polytropic equation of state for neutron stars

M. Berbel* and S. Serna

Universitat Autònoma de Barcelona, Bellaterra 08193, Spain

(Received 22 June 2023; accepted 15 September 2023; published 23 October 2023)

The equation of state (EoS) governing high-density matter inside neutron stars can exhibit phase transitions (PTs), which have the potential to induce anomalous wave structures in hydrodynamics and alterations in star stability. However, existing analytic models that are employed to replace realistic tabulated EoS in simulations often fall short in accurately capturing the intricate thermodynamics associated with these PT. Modeling PTs poses a challenge as they occur in thin density regions yet significantly impact the description of matter, rendering the EoS nonconvex and leading to a distinct hydrodynamic behavior. In this paper, we present a new analytic model for tabulated EoS with special focus on the modeling of PTs by means of a thermodynamically adaptive slope piecewise polytropic (T-ASPP) approximation, able to replicate nonconvex EoS and therefore triggering anomalous wave dynamics. In addition, we present a comprehensive analysis of the stellar properties (mass, radius, and tidal deformability) obtained from our model and compare them with those derived from the tabulated EoS. The results demonstrate that our T-ASPP EoS model provides a fair approximation to the neutron star properties. Furthermore, we investigate the hydrodynamic discrepancies between including and excluding the proper thermodynamics of PTs by examining two Riemann problems. This analysis sheds light on the significant impact of incorporating the accurate thermodynamics of PTs on the hydrodynamic behavior.

DOI: 10.1103/PhysRevD.108.083031

I. INTRODUCTION

The understanding of the equation of state (EoS) for matter beyond nuclear density remains a significant challenge in astrophysics. This highly dense matter is encountered in the cores of neutron stars (NSs), where thermal effects can be neglected rendering the EoS a relation between pressure and density, commonly referred to as a cold EoS. Various theoretical models have been proposed to describe the NS core, including nucleons, hyperons, or boson condensates, leading to increasingly complex EoS models that incorporate the corresponding microphysical descriptions. These models have been constrained through a combination of electromagnetic signal observations and heavy-ion collision experiments [1–3]. More recently, gravitational wave detections [4–7] have provided new insights and observational constraints.

One intriguing aspect of high-density matter is the possibility of phase transitions (PTs) to exotic states, such as quark-gluon plasma or the presence of hyperons. Although the nature of these PTs remains uncertain, they can significantly impact the stability [8,9] and dynamical evolution of NSs through hydrodynamics [10,11]. The study of PTs is often approached through the examination of the sound speed of the fluid c_s^2, which, in the case of a cold EoS, is given by the derivative of the pressure with respect to density.

Notably, the PT to quark-gluon plasma has been observed to induce a loss of monotonicity in the sound speed [12,13], which is otherwise expected to monotonically increase. Bedaque and Steiner [14] have concluded that the sound speed of high-density matter exhibits nonmonotonic regions.

The sound speed of the fluid is closely linked to the concept of the fundamental derivative [15], defined as

$$\mathcal{G} = 1 + \frac{\partial \ln(c_s)}{\partial \ln(\rho)}, \tag{1}$$

where ρ represents the rest-mass density. An EoS with a changing sign $\mathcal{G}$ is referred to as nonconvex.

A study of the effects of a nonconvex EoS describing the matter of NSs has been performed through a phenomenological Gaussian Gamma Law (GGL) EoS [16]. The GGL EoS presents a nonlinear adiabatic index, leading to nonmonotonic sound speed along a given region. This EoS was employed in hydrodynamics experiments considering special relativistic hydrodynamics [16,17] revealing the development of anomalous wave structure. Further numerical experiments on the stability and collapse of NSs [11] indicate that nonconvex EoS can accelerate the collapse

*marinaberbelp@gmail.com

into black holes and leave an imprint on the gravitational wave signal of the infalling phase.

Simulations involving NSs commonly employ analytic EoS models characterized by a few parameters. These computationally efficient models can adequately represent the realistic tabulated EoSs derived from the microphysics of the matter constituents. One widely utilized model is the piecewise polytropic (PP) approach proposed in [18], which employs four free parameters to effectively capture the high-density region of EoS of different natures. This approach provides a reasonable reconstruction of the pressure and yields stellar properties similar to those obtained from the tabulated data. The PP model has been successfully employed in simulations of NS binaries [19] and is implemented in several numerical codes involving NSs [20–24].

However, the PP model is limited in the representation of the thermodynamic properties of PTs. Given a polytrope for the pressure

$$P(\rho) = \kappa\rho^{\Gamma}, \tag{2}$$

the sound speed and the fundamental derivative are

$$c_s^2 = \kappa\Gamma\rho^{\Gamma-1}, \qquad \mathcal{G} = \frac{\Gamma+1}{2}. \tag{3}$$

Therefore, the sound speed is always monotonic, and the fundamental derivative has a constant, positive value. As a consequence, any PP model fails to be nonconvex.

In this paper, we propose an analytic EoS model for NSs that allows nonconvex regions. Following the approach of the PP model, we fit the pressure of tabulated EoSs with polytropes and change to a different definition at PTs to account for the different behavior of the pressure. We refer to our model as thermodynamically adaptive slope piecewise polytropic approximation (T-ASPP). First, we describe a methodology to locate PTs in tabulated EoS. Then, we design an analytic model for the EoS at PTs that can be seamlessly stitched to any pressure model outside PTs ensuring a continuous EoS. This PT model allows for the presence of negative values of the fundamental derivative and, therefore, is capable of representing nonconvex EoS. The T-ASPP EoS model uses this reconstruction for PTs and polytropes outside them. Different polytropes are partitioned according to the thermodynamic properties of the tabulated data. We provide graphical examples of the fitting of T-ASPP in comparison with PP approximation and show the discrepancy that both models have on stellar properties with respect to tabulated EoS. We include examples of hydrodynamics that illustrate the different wave structure arising from the PP and T-ASPP model due to the presence of a nonconvex region.

The paper is organized as follows. In Sec. II, we present a methodology for detecting PTs in tabulated EoS. Section III introduces a model for matter at PTs. Complementing the model for PTs, Sec. IV describes a polytropic fit of the pressure outside PTs, altogether constructing our T-ASPP model. Finally, in Sec. V, we illustrate the performance of our T-ASPP model by comparing it with the PP approximation. In Sec. VI, we draw our conclusions.

II. DETECTING PHASE TRANSITIONS

PTs of matter are characterized by an abrupt change in its thermodynamic properties. Along PTs, more than one phase coexists, and matter deviates from its usual behavior in pure phases. In a mixed phase, the slope of pressure with density decreases with respect to the slope in pure phases. The main affected quantities relate to the derivatives of the pressure.

In a cold EoS, where the entropy is constant, the sound speed is defined as

$$c_s^2 = \frac{\partial P}{\partial \rho}. \tag{4}$$

Along PTs, the sound speed decreases, presenting a local minimum.

The adiabatic exponent,

$$\gamma = \frac{\rho}{P}\frac{\partial P}{\partial \rho}, \tag{5}$$

presents a kink (discontinuity in first derivative) at the start of a PT, while it is a smooth quantity along pure phases [25].

The key behavior identifying a PT is the break of monotonicity of the sound speed which in turn induces the kink in the adiabatic exponent. We use these features to identify the start of PTs in tabulated EoS. We consider that the PT is over and matter is in a pure phase when these thermodynamic quantities recover their usual smooth behavior.

To obtain the sound speed and adiabatic exponent from a tabulated EoS containing values on density ρ and pressure P, we use the derivative of a three-point Lagrangian interpolation, as it allows for unevenly spaced data. Given consecutive abscissa points $[x_0, x_1, x_2]$ with corresponding $[y_0, y_1, y_2]$ ordinate values, then

$$\frac{\partial y}{\partial x} \approx \frac{y_0(2x - x_1 - x_2)}{(x_0 - x_1)(x_0 - x_2)} - y_1\frac{2x - x_0 - x_2}{(x_0 - x_1)(x_1 - x_2)} + y_2\frac{2x - x_0 - x_1}{(x_0 - x_2)(x_1 - x_2)}. \tag{6}$$

Because of the numerical nature of the values in the tables, the points contain an intrinsic error that may lead to oscillations in the numerical derivatives. These oscillations need to be distinguished from actual properties of the fluid.

TABLE I. Density values of the extremes of the PTs located in EoS tables from Arizona [27]. Density is presented in 10^{14} g/cm^3. Notice that the densities have been rounded for the table to fit in the page.

	PT1		PT2		PT3		PT4	
EoS	ρ_L	ρ_R	ρ_L	ρ_R	ρ_L	ρ_R	ρ_L	ρ_R
PS	3.645	7.458						
GS1	4.316	9.557						
GS2	4.648	8.587						
BGN1H1	6.142	11.62						
H4	5.013	6.109	6.839	7.370	11.39	12.02	14.48	17.297
H5	5.511	7.072	7.935	8.632	15.84	16.57		
H6	4.847	6.341	6.773	7.603	10.79	12.28		
H7	5.777	7.204	8.366	8.898	16.14	16.57		
ALF1	3.735	7.091						
ALF2	4.210	6.350						

The challenges come from detecting a kink in the discrete adiabatic exponent in a general manner and determining that the sound speed is varying smoothly after the PT. For this purpose, we introduce the use of the total variation (TV).

The TV is a measure of oscillatory behavior. For a set of discrete values $\{u_i\}_{i=0}^m$, it is defined as

$$TV(u) = \sum_{i=0}^{m-1} |u_{i+1} - u_i|. \tag{7}$$

A strategy to detect kinks, used in [26], is to define the *local total variation* (LTV) of n points at the value of index j as

$$TV_j^n(u) = \sum_{i=j}^{j+n} |u_{i+1} - u_i|. \tag{8}$$

This quantity measures how much the magnitude u is changing around the point of index j. If the magnitude varies smoothly, the value of $TV_j^n(u)$ is similar for consecutive j and fixed n. If there is an abrupt change like a kink in the magnitude, then the LTV increases.

To detect a kink in the adiabatic exponent, we compute $TV_j^3(\gamma)$ for every point in the table. The selection $n = 3$ is made to keep the study very local, as PTs extend for small regions of density. Including more points can mix them with pure phases covering up their effects. A kink introduces a local maximum in the sequence of LTVs.

For a tabulated EoS including the sound speed and adiabatic exponent, which can be calculated from the pressure and density values as specified above, we propose the following criteria to identify a PT:

(i) A PT starts at ρ_j if the corresponding value of the sound speed is a local maximum. To avoid misclassifying oscillations, we require that the sound speed decreases for at least two consecutive data points. In addition, the start of the PT must induce a kink in the adiabatic exponent, which implies a local maximum in its LTV. This maximum can occur at index $j-1$, j, or $j+1$. The actual position of the maximum is determined from how the numerical derivatives were calculated during the construction of the table.

(ii) A PT finishes at ρ_q if the sound speed is larger than or equal to the value it had at the beginning of the PT, since the sound speed is always larger in pure phases than in mixed phases. Also, c_s^2 should increase monotonically and smoothly. We require $TV_q^3(c_s^2)$ to be less than or equal to $TV_j^3(c_s^2)$, implying that the sound speed is smoother than when it suddenly changed at the start of the PT.

We apply the method described to locate PTs in tabulated EoS to the tables taken from Arizona University NS EoS database [27]. The EoS that present at least one PT are PS [28], GS1-GS2 [29], BGN1H1 [30], H4-H7 [31], and ALF1-ALF2 [32]. The left and right extremes of the PTs are gathered in Table I.

The PTs located lie at the transition between the crust and the core of the NS, representing the change from solid to liquid matter. The EoS models H4-H7 present additional PTs deep into the core related to the progressive addition of hyperon species.

III. MODELING PHASE TRANSITIONS

In this section, we focus on the modeling of the EoS along PTs, assuming there exists another modeling for the pressure outside them. We will refer to such a model as $P_{\text{fit}}(\rho)$ during this section.

To accurately represent the thermodynamic properties of a PT, we model the sound speed (4) of the fluid. This choice is motivated by the fact that the sound speed exhibits distinct behavior along PTs, characterized by a change in monotonicity and the presence of a local minimum.

Let $\mathcal{C}(\rho)$ represent the curve obtained by modeling the sound speed of a tabulated EoS. Starting from an initial state (ρ_i, P_i), we can express the pressure as

$$P(\rho) = P_i + \int_{\rho_i}^{\rho} \mathcal{C}(t)\mathrm{d}t. \tag{9}$$

Additionally, we can derive an expression for the internal energy. Since we are considering a cold EoS, where the entropy is constant, the first law of thermodynamics leads to

$$\varepsilon(\rho) = \varepsilon_i + \int_{\rho_i}^{\rho} \frac{P(t)}{t^2}\mathrm{d}t. \tag{10}$$

To model the sound speed across the PT, we suggest using a polynomial of degree n,

$$pn(\rho) = \sum_{i=0}^{n} a_i \left(\frac{\rho}{\rho_m}\right)^i, \tag{11}$$

where we restrict the values of n to $\{2,3,4\}$. A linear approximation ($n = 1$) fails to capture the change in monotonicity during the PT, while higher degrees ($n > 4$) may introduce unrealistic behavior, as discussed later. The parameter ρ_m represents a density scale factor, and its value is chosen to be the density at which the minimum sound speed occurs during the PT. Finally, a_i denote the free parameters of the model.

Given an interval for the PT, $[\rho_L, \rho_R]$, we ensure continuity of pressure at ρ_L by selecting $\rho_i = \rho_L$, $P_i = P_L = P_{\mathrm{fit}}(\rho_L)$ in (9).

Continuity at ρ_R is imposed by equating $P_{\mathrm{fit}}(\rho_R) = P_{pn}(\rho_R) = P_R$:

$$P_R = P_L + \sum_{i=0}^{n} \frac{a_i}{(i+1)\rho_m^i}(\rho_R^{i+1} - \rho_L^{i+1}). \tag{12}$$

To satisfy this condition, we fix one of the free parameters, a_0, as follows:

$$a_0 = \underbrace{\frac{P_R - P_L}{\rho_R - \rho_L}}_{d} - \sum_{i=1}^{n} \frac{a_i}{\rho_m^i} \underbrace{\frac{\rho_R^{i+1} - \rho_L^{i+1}}{(i+1)(\rho_R - \rho_L)}}_{\theta_i}. \tag{13}$$

Our model, when including continuity of pressure, presents an independent term d given by the extremes of the PT and a constant factor θ_i multiplied by each of the remaining free parameters of the model:

$$pn(\rho) = \sum_{i=1}^{n} \frac{a_i}{\rho_m^i}(\rho^i - \theta_i) + d. \tag{14}$$

Pressure and internal energy values are obtained straightforwardly:

$$P(\rho) = P_L + \sum_{i=1}^{n} \frac{a_i}{\rho_m^i}\left(\frac{\rho^{i+1} - \rho_L^{i+1}}{i+1} - \theta_i(\rho - \rho_L)\right) + d(\rho - \rho_L), \tag{15}$$

$$\varepsilon(\rho) = \varepsilon_L + \sum_{i=1}^{n} \frac{a_i}{i(i+1)\rho_m^i \rho}(i\rho_L^{i+1} - (i+1)\rho_L^i \rho + \rho^{i+1} + (i+1)i\theta_i(\rho \ln(\rho_L/\rho) + \rho - \rho_L)) + d\left(\ln(\rho/\rho_L) + \frac{\rho_L - \rho}{\rho}\right) - \frac{P_L(\rho_L - \rho)}{\rho_L \rho}. \tag{16}$$

Once a PT is localized, we have the density values of its extremes, ρ_L and ρ_R, as well as the corresponding sound speed values, c_L and c_R. Additionally, inside the transition region, we can identify the sound speed's minimum c_m at density ρ_m. Moreover, it is known that at ρ_L there exists a local maximum of the sound speed indicating the onset of the PT. We can impose these pairs of values and local extrema on our model to determine the free parameters.

We have a total of five conditions (three pairs of values, two extrema), and we can impose a maximum of n conditions simultaneously on each model. This leads to a set of parametrizations from which we can choose the most appropriate one. It is important to note that for $n = 2$ our model takes the form of a parabola and therefore it only makes sense to impose the minimum as its vertex.

Given a tabulated EoS and a PT location within, we calculate all parametrizations for $n = 2$, 3, 4. We discard those that are not causal or thermodynamically consistent. After eliminating parametrizations that contradict physically valid EoS, we further filter them based on their agreement with the behavior of the sound speed along a PT. We only consider parametrizations with exactly one local minimum as the sole extreme within the PT interval. This filtering process usually excludes higher-order polynomials since they tend to exhibit additional extrema along the PT.

The remaining parametrizations are physically consistent models for the PT. To select the more appropriate one among them, we consider the error of a model as the average between the relative errors of pressure and sound speed. The parametrization with smaller error is the model for the PT. This approach allows us to choose the best fitting polynomial without introducing additional free parameters into the overall EoS model.

IV. THERMODYNAMICALLY ADAPTIVE SLOPE PIECEWISE POLYTROPIC APPROXIMATION

To construct an expression for the pressure outside the PTs, we follow the idea in [18] to fit polytropes with the tabulated data. A polytrope is defined as (2), where κ and Γ are the free parameters of the model. The internal energy and other thermodynamic quantities for polytropes are detailed in Sec. III of [18].

Since PTs are modeled independently, we remove these regions of data from the tabulated EoS. The outcome is a table with gaps that separate different polytropes, a total of the number of PTs plus one. The dividing densities therefore arise from the thermodynamics, and the polytropes adjust smoother data, which does not contain the different slope of the pressure along PTs.

We consider that the crust of the NS is described by the four fixed polytropes indicated in [18]. Our modeling applies beyond their last dividing density and continues the crust at some matching density. If the tabulated EoS presents PTs along the crust, our modeling approach can be applied to the whole NS.

A first polytrope, marked with subindex 1, matches the model of the crust, with subindex c, at some density ρ_1 and extends up to the start of the first PT of the EoS. To ensure continuity of the pressure, the free parameters of the first polytrope are the matching density ρ_1 and the adiabatic index Γ_1. The matching density determines $\kappa_1 = \kappa_c \rho_1^{\Gamma_c - \Gamma_1}$. To fit the relation, we minimize the root-mean-squared residual

$$S_1 = \sqrt{\frac{1}{m} \sum_{\rho_i > \rho_1} (\log(P_i) - \log(\kappa_c \rho_1^{\Gamma_c - \Gamma_1}) - \Gamma_1 \log(\rho_i))^2}, \tag{17}$$

where m is the number of density points above the value ρ_1.

Polytropes defined in the region after a PT do not require continuity conditions with any other piece, and therefore both parameters κ and Γ can be used in the fitting. The cost function to minimize is

$$S_2 = \sqrt{\frac{1}{N} \sum_{\rho_i} (\log(P_i) - \log(\kappa) - \Gamma \log(\rho_i))^2}, \tag{18}$$

where N is the number of points in the corresponding tabulated data.

Given that the high-density regime of the EoS is adjusted with a number of polytropes equal to the number of PTs plus one, an accurate reconstruction of the pressure is achieved when multiple PTs are present. Nevertheless, in the presence of a single PT, one polytrope may not adequately capture the variations in pressure slope within the stellar core. To address this issue, we design a procedure to locate significant changes in the slope of pressure within the tabulated data that would indicate an appropriate matching density between two polytropes modeling the core. The method is designed to be applied to EoS with a single PT and focuses on the region after it.

A. Locating significant changes of the pressure slope

When trying to fit the whole core of a NS with a single polytrope an average slope of the tabulated states is captured, not being very accurate neither in the outer nor the inner core. We propose using two polytropes instead. The matching density is chosen based on the behavior of the pressure, analyzed through the sound speed.

We define a significant change of slope as a jump discontinuity of the sound speed or a decreasing region that is not a PT. If there is no significant change of slope, the pressure can be accurately fitted with a single polytrope. If one of these phenomena takes place, it indicates the matching density between the two polytropes. If both types of changes defined happen in a tabulated EoS, we prioritize as matching density the position of the jump discontinuity.

We look for local maxima in the data to locate a decreasing region of the sound speed. We impose that the sound speed decreases for at least two data points after the maximum to avoid oscillatory behavior. If there is more than one maximum, we consider as matching density the one at a smaller density.

To locate a jump discontinuity in the sound speed, we use the LTV defined in Eq. (8), $TV_j^3(c_s^2)$. We compute this quantity for the whole region after the PT and look for maxima of the LTV. We consider a maximum of the LTV relevant if its value is larger than the mean of the LTV along the region plus two times the standard deviation. In a Gaussian distribution, this criterion isolates the data outlier from the mean with 95% confidence. We consider that this general fact can be extended to our study and the criterion identifies peaks of the LTV that are actually significant jumps in the sound speed. If there is more than one peak obeying this criterion, the matching density from this approach is the density value with the larger LTV.

When the region after the PT is fitted with two different polytropes, 2 and 3, separated at density ρ_c selected with the method above, then the first polytrope has two free parameters and is fitted optimizing cost S_2 (18) using densities up to ρ_c. To ensure continuity of the pressure at ρ_c, the second polytrope has a single free parameter, Γ_3 and $\kappa_3 = \kappa_2 \rho_c^{\Gamma_2 - \Gamma_3}$. Therefore, the cost function to minimize for its fitting is

$$S_3 = \sqrt{\frac{1}{N} \sum_{\rho_i > \rho_c} (\log(P_i) - \log(\kappa_2 \rho_c^{\Gamma_2 - \Gamma_3}) - \Gamma_3 \log(\rho_i))^2}. \tag{19}$$

Our analytic model for tabulated EoS utilizes polynomials to model PTs, capturing the different thermodynamic behavior of these regions. It employs polytropes to fit the pressure in terms of the density when the slope is smooth, and it detects the need of more polytropes for an accurate fit analyzing the slope of the pressure. Therefore, the model adapts the slope of the pressure attending to the thermodynamic properties of the tabulated data.

The process to construct the T-ASPP model of a tabulated EoS can be summarized as follows:

(1) Locate PTs in the tabulated EoS analyzing the sound speed and adiabatic index (see Sec. II).
(2) Fit polytropes for every region of tabulated data outside PTs. Locate the need of additional polytropes by analyzing the changes of the pressure slope (see Sec. IV).
(3) Construct polynomial models at PTs given the pressure values at their extremes evaluated with the polytropes. Select the polynomial model that is causal and thermodynamically consistent, presenting a single minimum and the least relative error in the sound speed and pressure (see Sec. III).

V. MODEL COMPARISON

We compare the performance of our T-ASPP model with the PP approximation. We present the difference on mass, radius, and dimensionless tidal deformability of both models with respect to the results from the tabular data. We also illustrate the difference on the hydrodynamic evolution when using the two models by solving some test problems for a particular EoS.

A. Stellar properties

We compute the mass, radius, and tidal deformability for a sequence of NSs ranging from the central density of the maximum mass NS according to the tabulated EoS down to the central density where the NS reaches a 16 km radius. This is a conservative approach to the maximum possible value estimated for a NS [33,34].

For the sequence of stars obtained from each EoS model, we compute the relative percent difference (RPD), $(\text{average}|X_{\text{model}}/X_{\text{tab}} - 1|)100$, of the stated stellar properties with respect to the tabulated EoS. In this way, we compare the performance in the representation of NSs all over the stable branch. The results are gathered in Table II.

We consider the ten EoS with PTs from the 34 analyzed. The T-ASPP model reduces the error of the PP approximation in five EoS for the mass (GS2, BGN1H1, H6, ALF1, and ALF2), six for the radius (PS, GS1, GS2, H4, H6, and ALF1), and six for the tidal deformability (PS, GS2, H5, H7, ALF1, and ALF2). For the EoS that are not improved, the performance is similar.

In particular, EoS ALF1 and ALF2 present a large improvement with T-ASPP model with respect to the PP, reducing noticeably the error for the three stellar properties (the error for ALF2 radius is similar for both models). In the T-ASPP model, the polytrope after the PT captures better the behavior of the tabulated data than in the PP model, where it is influenced by the different slope along the PT. Moreover, T-ASPP presents a third polytrope for the higher densities starting at a dividing density larger than the one of the PP. Since the division is done in a state marking a change of slope, the following polytrope resembles better the tabulated EoS.

Figure 1 presents the modeling of the tabulated PS EoS around its PT, showcasing the tabulated data against PP and T-ASPP models. In the pictures, we show from top to bottom pressure, sound speed, and fundamental derivative. Although the RPD in mass is larger than with the PP model, T-ASPP decreases the error in radius and tidal deformability. The pressure is much better reconstructed with T-ASPP since it captures the different slope. This fact is appreciated in the sound speed. Along the PT, the T-ASPP model decreases and recovers smoothly, while the PP model presents a jump discontinuity. The fundamental derivative shows that, according to the tabulated data, PS EoS is nonconvex (the fundamental derivative changes sign). Both PP and T-ASPP models fail to reproduce that behavior. We include the necessary parameters to construct the T-ASPP model for PS EoS in Table IV.

In Fig. 2, we depict pressure, sound speed, and fundamental derivative for the ALF1 EoS presenting the tabulated data and both PP and T-ASPP models. Although the pressure is reconstructed similarly by both analytic models, the sound speed is quite different. Along the PT, the PP model presents a jump discontinuity of increasing sound speed, while T-ASPP has a nonmonotonic shape. The thermodynamically more accurate reconstruction of the T-ASPP in this region induces the nonconvex region

TABLE II. RPD of mass (M), radius (R), and dimensionless tidal deformability (Λ) with respect to the tabulated EoS for different EoS.

	RPD M		RPD R		RPD Λ	
EoS	PP	T-ASPP	PP	T-ASPP	PP	T-ASPP
PS	1.185	2.187	3.019	0.7440	9.143	8.732
GS1	2.133	2.481	2.429	1.298	15.61	18.66
GS2	2.386	1.621	2.087	1.046	16.16	15.84
BGN1H1	3.888	2.562	0.856	1.100	26.80	36.73
H4	1.217	1.287	3.268	3.256	6.056	6.304
H5	1.520	2.383	1.918	2.663	28.10	26.55
H6	1.474	1.373	1.883	1.488	32.748	33.79
H7	1.447	1.910	3.007	3.511	26.24	25.58
ALF1	6.191	3.810	2.705	1.053	34.09	23.00
ALF2	8.783	6.815	3.268	3.298	44.33	31.289

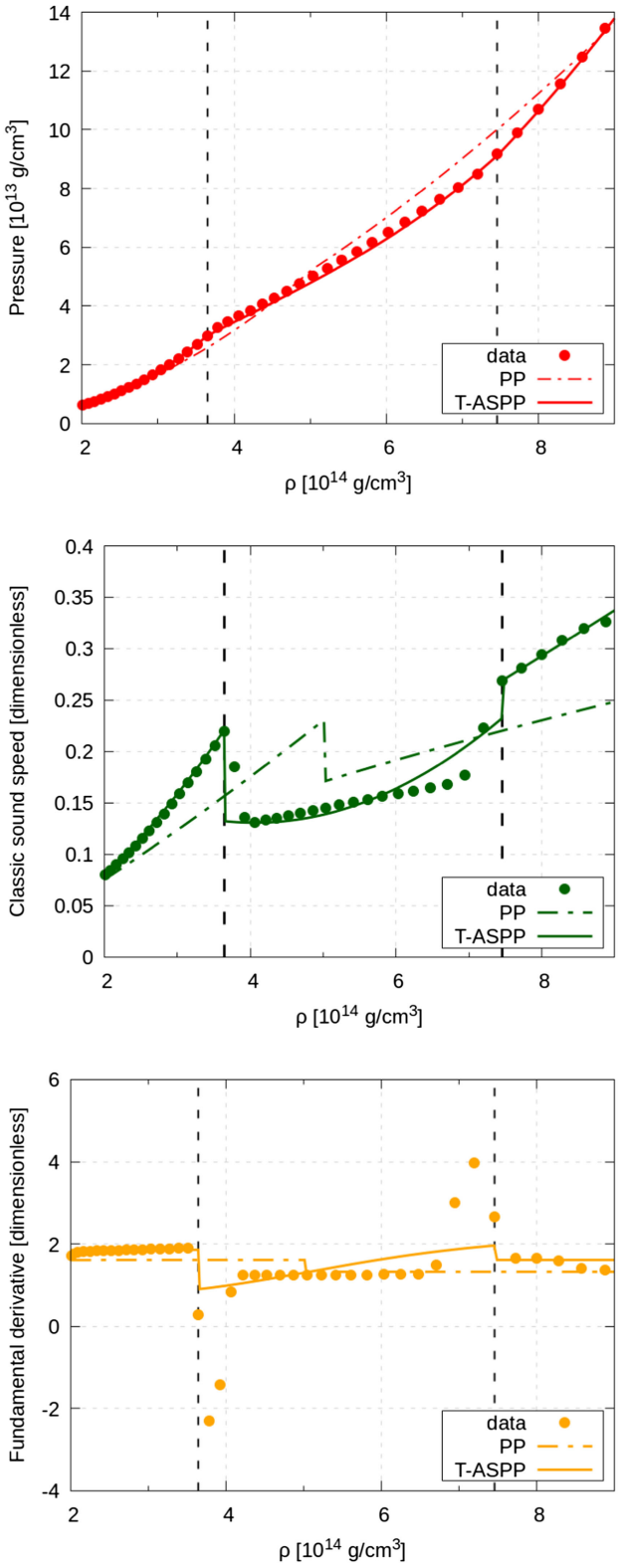

FIG. 1. Region around the PT, marked in black vertical lines, for PS EoS. Tabulated data in points, fit by PP model in dashed line, T-ASPP model in continuous line. From top to bottom: pressure, fluid sound speed, and fundamental derivative.

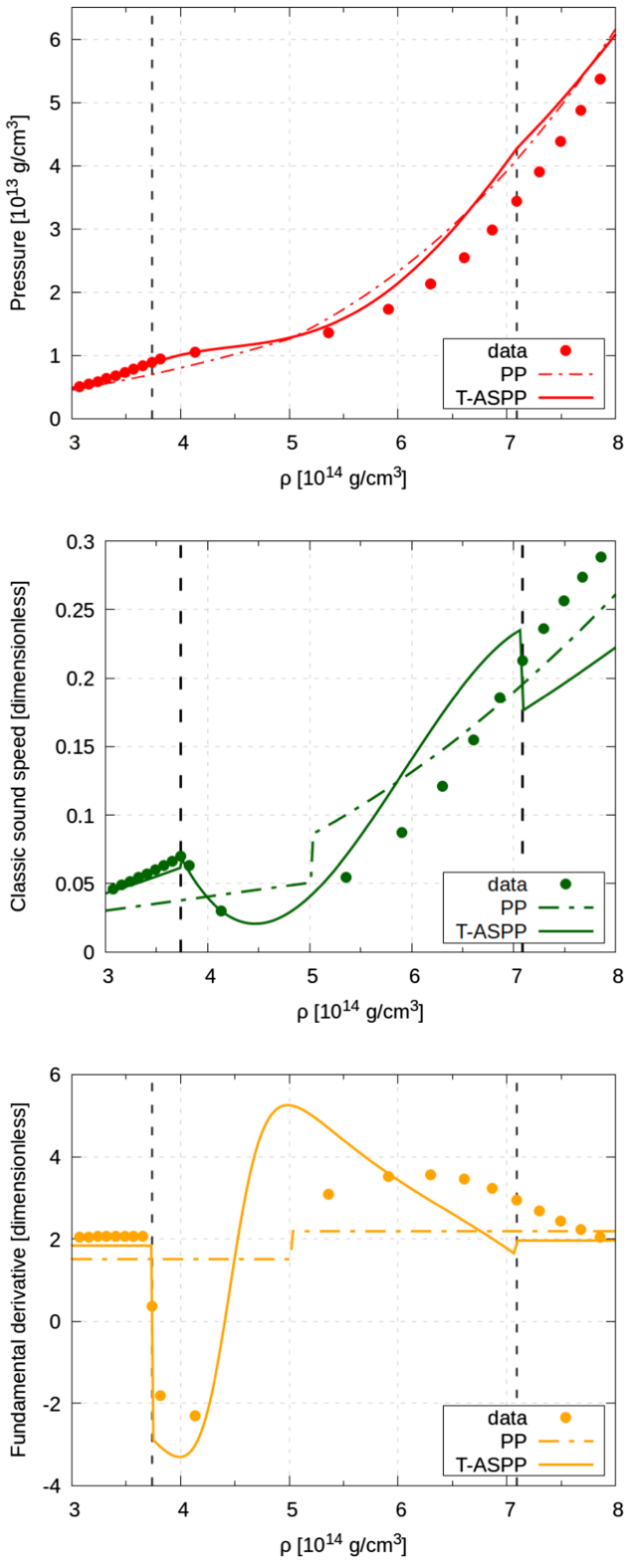

FIG. 2. Region around the PT, marked in black vertical lines, for ALF1 EoS. Tabulated data in points, fit by PP model in dashed line, T-ASPP model in continuous line. From top to bottom: pressure, fluid sound speed, and fundamental derivative.

TABLE III. Riemann problems designed for ALF1 EoS.

	ρ_L (g/cm^3)	v_L	ρ_R (g/cm^3)	v_R
Cold blast wave 1	8×10^{13}	0	4.3×10^{14}	0
Cold blast wave 2	3.1×10^{14}	0	4.45×10^{14}	0

TABLE IV. Summary of T-ASPP model for PS EoS. Density limits ρ_s (starting density) and ρ_e (ending density) are in g/cm^3. Quantities marked with the symbol * have been obtained with the methods proposed above. The other quantities are obtained from literature or continuity conditions.

Polytropes	Crust from [18]	$\rho_s = 0$	$\rho_e = 2.44034e7$	$\kappa = 6.8011e\text{-}9$	$\Gamma = 1.58425$
		$\rho_s = 2.44034e7$	$\rho_e = 3.78358e11$	$\kappa = 1.06186e\text{-}6$	$\Gamma = 1.28733$
		$\rho_s = 3.78358e11$	$\rho_e = 2.62780e12$	$\kappa = 53.2697$	$\Gamma = 0.62223$
		$\rho_s = 2.62780e12$	$*\rho_e = 5.408342e13$	$\kappa = 3.99874e\text{-}8$	$\Gamma = 1.35692$
	High density	$*\rho_s = 5.408342e13$	$*\rho_e = 3.6452604e14$	$\kappa = 1.407284e\text{-}26$	$*\Gamma = 2.700651$
		$*\rho_s = 7.4578e14$		$*\kappa = 1.678417e\text{-}19$	$*\Gamma = 2.201028$
PT polynomial		$*\rho_s = 3.6452604e14$	$*\rho_e = 7.4578e14$	$*\rho_m = 4.0628832e14$	
		$*a_1 = -0.291327$	$* a_2 = 0.145664$	$*a_3 = 0$	$*a_4 = 0$

indicated by the tabulated data. We include the necessary parameters to construct the T-ASPP model for ALF1 EoS in Table V.

In general, our T-ASPP model fairly represents the stellar properties of NSs. Although it may contain more free parameters than the PP model, in the case of several PTs within the high-density region of the EoS, the analytic expression is equally simple and computationally efficient. It also presents the advantage of a more accurate representation of the thermodynamics, depicting regions of smooth decrease of the sound speed and allowing for nonconvex EoS models.

B. Hydrodynamics

With the aim of showcasing the impact of PTs on the fluid hydrodynamic evolution, we design two Riemann problems for special relativistic hydrodynamics. Using PP and T-ASPP models for ALF1 EoS, we present examples that reveal the impact of an accurate thermodynamics.

We design blast wave problems [35] to use with cold EoS. The Riemann problems suggested, cold blast wave 1 and 2, are gathered in Table III. Notice that the initial value for the density determines the initial value of the pressure. Therefore, the initial state of pressure may be different for different modelings of the same EoS. Using the spatial domain $x \in [0, 1]$ with initial discontinuity at $x = 0.5$, we present the solution profile for density and fundamental derivative at time $t_f = 0.2$. We perform numerical simulations using the scheme in [17], which is able to handle nonconvex dynamics in relativistic scenarios. The graphics are displayed in $x \in [0.4, 0.6]$, focused on the waves.

Figure 3 shows the solution for the cold blast wave problem 1 using PP and T-ASPP models. The left initial condition is outside the PT of the EoS, while the right initial condition is inside. For the PP model, the problem develops within a single polytropic definition of the EoS, while for T-ASPP, it traverses the end of the crust, a first polytrope and part of the polynomial modeling the PT. The three different definitions can be appreciated in the fundamental derivative picture since the quantity presents jump discontinuities. For the PP model, we observe an expansive rarefaction moving to the right and a compressive shock moving to the left, a structure intrinsic of convex dynamics. For T-ASPP model, however, there is a change of sign of the fundamental derivative along the solution of the Riemann problem inducing nonconvex dynamics. While the wave to the left is still a shock wave, the wave to the right traverses the negative region of the fundamental derivative breaking into a composite wave. A shock attached to a rarefaction moves toward the right.

We present the solution for the cold blast wave 2 using PP and T-ASPP models in Fig. 4. In this case, the left initial condition is closer to the PT, and the solution for the T-ASPP model only traverses part of the polynomial definition and a polytrope before. The PP presents an expansive rarefaction toward the right and a compressive shock to the left. T-ASPP model presents shock waves moving in both directions. This is due to the change of sign of the fundamental derivative during the development of the right wave.

VI. CONCLUSIONS

We have presented a methodology for the detection and modeling of phase transitions in realistic tabulated

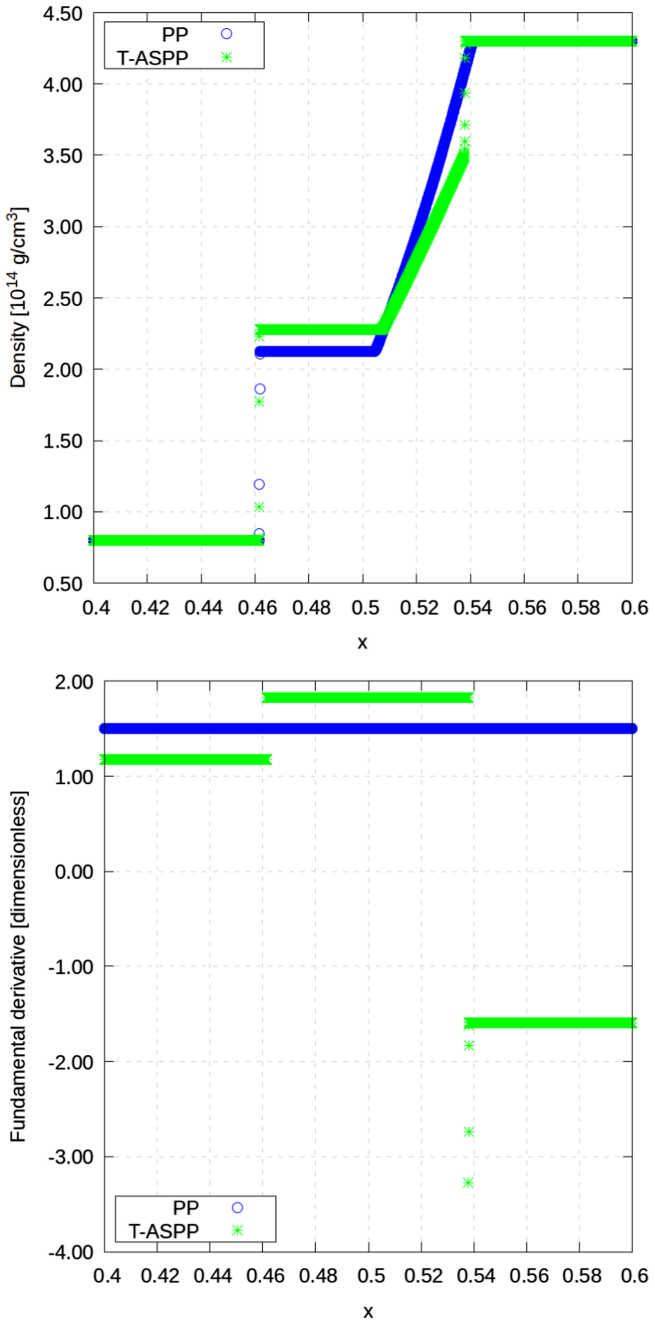

FIG. 3. Numerical solution of cold blast wave 1 at time $t = 0.2$ using ALF1 EoS. In dots, there is the solution using the PP model for the EoS. In crosses, there is the solution using the T-ASPP model.

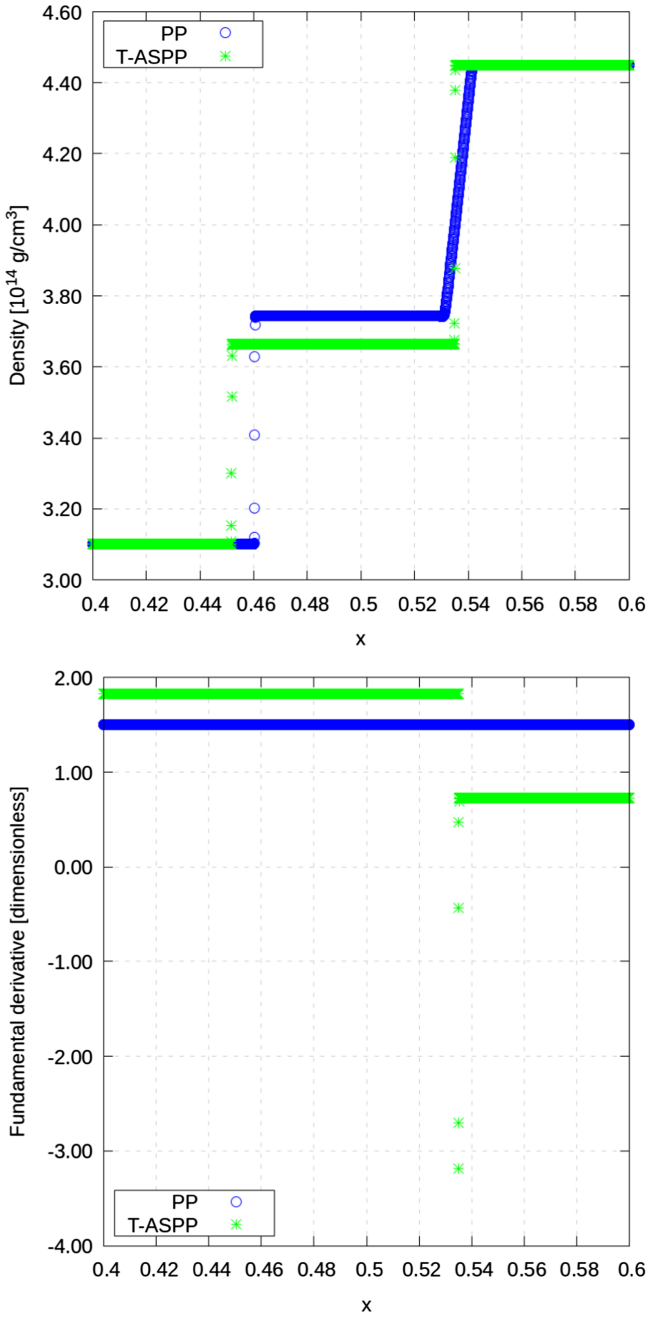

FIG. 4. Numerical solution of cold blast wave 2 at time $t = 0.2$ using ALF1 EoS. In dots, there is the solution using the PP model for the EoS. In crosses, there is the solution using the T-ASPP model.

EoS for NS. Our approach, the T-ASPP approximation, incorporates a polynomial representation of PTs within an overall piecewise polytropic EoS. By employing this methodology, we have been able to capture the nonconvex behavior of EoS associated with PTs, enabling the emergence of anomalous wave structures in hydrodynamics.

Our analysis of the stellar properties, encompassing mass, radius, and tidal deformability, demonstrates the effectiveness of the T-ASPP model in providing a reliable approximation of NS properties derived from tabulated EoS. The examination of hydrodynamic behavior through the investigation of two Riemann problems highlights the substantial impact that accurate incorporation of the PT thermodynamics can have.

TABLE V. Summary of T-ASPP model for ALF1 EoS. Density limits ρ_s (starting density) and ρ_e (ending density) are in g/cm^3. Quantities marked with the symbol * have been obtained with the methods proposed above. The other quantities are obtained from literature or continuity conditions.

Polytropes	Crust from [18]	$\rho_s = 0$	$\rho_e = 2.44034e7$	$\kappa = 6.8011e\text{-}9$	$\Gamma = 1.58425$
		$\rho_s = 2.44034e7$	$\rho_e = 3.78358e11$	$\kappa = 1.06186e\text{-}6$	$\Gamma = 1.28733$
		$\rho_s = 3.78358e11$	$\rho_e = 2.62780e12$	$\kappa = 53.2697$	$\Gamma = 0.62223$
		$\rho_s = 2.62780e12$	$*\rho_e = 5.408342e13$	$\kappa = 3.99874e\text{-}8$	$\Gamma = 1.35692$
	High density	$*\rho_s = 1.390908e14$	$*\rho_e = 3.735e14$	$\kappa = 1.31538e\text{-}26$	$*\Gamma = 2.663749$
		$*\rho_s = 7.0906e14$	$*\rho_e = 1.423560e15$	$*\kappa = 1.51574e\text{-}30$	$*\Gamma = 2.925772$
		$*\rho_s = 1.423560e15$		$\kappa = 7.56645e\text{-}09$	$*\Gamma = 1.493853$
PT polynomial		$*\rho_s = 3.735e14$	$*\rho_e = 7.0906e14$	$*\rho_m = 4.1347446e14$	
		$*a_1 = -7.368422$	$*a_2 = 5.477297$	$*a_3 = -1.275412$	$*a_4 = 0$

ACKNOWLEDGMENTS

This work was partially supported by the Spanish Government Grant No. PID2020–118236GB-I00.

[1] N. K. Glendenning, *Compact Stars: Nuclear Physics, Particle Physics and General Relativity* (Springer Science & Business Media, New York, 2012).
[2] H. Heiselberg and M. Hjorth-Jensen, Phys. Rep. **328**, 237 (2000).
[3] P. Hansel, A. Y. Potekhin, and D. G. Yakovlev, *Neutron Stars 1: Equation of State and Structure*, Astrophysics and Space Science Library (Springer, New York, NY, 2007).
[4] B. P. Abbott *et al.* (LIGO Scientific and Virgo Collaborations), Phys. Rev. Lett. **119**, 141101 (2017).
[5] B. P. Abbott *et al.* (LIGO Scientific and Virgo Collaborations), Phys. Rev. Lett. **119**, 161101 (2017).
[6] B. P. Abbott *et al.* (LIGO Scientific and Virgo Collaborations), Astrophys. J. Lett. **848**, L12 (2017).
[7] B. P. Abbott *et al.* (LIGO Scientific and Virgo Collaborations), Phys. Rev. Lett. **118**, 221101 (2017).
[8] J. Zdunik and P. Haensel, Astron. Astrophys. **551**, A61 (2013).
[9] I. Bednarek, P. Haensel, J. L. Zdunik, M. Bejger, and R. Mańka, Astron. Astrophys. **543**, A157 (2012).
[10] B. Peres, M. Oertel, and J. Novak, Phys. Rev. D **87**, 043006 (2013).
[11] A. Aloy, J. M Ibáñez, N.Sanchis-Gual, Martin Obergaulinger, J. A Font, S. Serna, and A. Marquina, Mon. Not. R. Astron. Soc. **484**, 4980 (2019).
[12] A. Bazavov *et al.*, Phys. Rev. D **90**, 094503 (2014).
[13] S. Borsányi, Z. Fodor, C. Hoelbling, S. D. Katz, S. Krieg, and K. K. Szabó, Phys. Lett. B **730**, 99 (2014).
[14] P. Bedaque and A. W. Steiner, Phys. Rev. Lett. **114**, 031103 (2015).
[15] P. A. Thompson, Phys. Fluids **14**, 1843 (1971).
[16] J. M. Ibáñez, A. Marquina, S. Serna, M. A. Aloy, Mon. Not. R. Astron. Soc. **476**, 1100 (2018).
[17] A. Marquina, S. Serna, and J. M. Ibáñez, J. Sci. Comput. **81**, 2132 (2019).
[18] J. S. Read, B. D. Lackey, B. J. Owen, and J. L. Friedman, Phys. Rev. D **79**, 124032 (2009).
[19] T. Dietrich, D. Radice, S. Bernuzzi, F. Zappa, A. Perego, B. Brügmann, S. V. Chaurasia, R. Dudi, W. Tichy, and M. Ujevic, Classical Quantum Gravity **35**, 24LT01 (2018).
[20] Einstein Toolkit: Open software for relativistic astrophysics, http://einsteintoolkit.org/.
[21] F. Löffler *et al.*, Classical Quantum Gravity **29**, 115001 (2012).
[22] P. Mösta *et al.*, Classical Quantum Gravity **31**, 015005 (2014).
[23] Langage Objet pour la RElativité NumériquE, https://lorene.obspm.fr/.
[24] RNS, http://www.gravity.phys.uwm.edu/rns.
[25] R. Menikoff and B. J. Plohr, Rev. Mod. Phys. **61**, 75 (1989).
[26] A. Marquina, SIAM J. Sci. Comput. **15**, 892 (1994).
[27] Neutron Stars—University of Arizona, http://xtreme.as.arizona.edu, tables retrieved January 2022.
[28] V. R. Pandharipande and R. A. Smith, Nucl. Phys. **A237**, 507 (1975).
[29] N. K. Glendenning and J. Schaffner-Bielich, Phys. Rev. C **60**, 025803 (1999).
[30] S. Balberg and A. Gal, Nucl. Phys. **A625**, 435 (1997).
[31] B. D. Lackey, M. Nayyar, and B. J. Owen, Phys. Rev. D **73**, 024021 (2006).
[32] M. Alford, M. Braby, M. Paris, and S. Reddy, Astrophys. J. **629**, 969 (2005).
[33] T. Riley *et al.*, Astrophys. J. Lett. **918**, L27 (2021).
[34] C. Drischler, S. Han, J. M. Lattimer, M. Prakash, S. Reddy, and T. Zhao, Phys. Rev. C **103**, 045808 (2021).
[35] M. L. Norman and K. H. A. Winkler, in *Astrophysical Radiation Hydrodynamics* (Springer, New York, 1986), pp. 449–476.